



1 Fractal behavior of soil water storage at multiple depths

2 Wenjun Ji¹, Mi Lin¹, Asim Biswas^{1*}, Bing C. Si², Henry W. Chau³, and Hamish P. Cresswell⁴

3 ¹ Department of Natural Resource Sciences, McGill University, 21111 Lakeshore Road, Ste-Anne-de-
4 Bellevue, Quebec, Canada, H9X3V9

5 ² Department of Soil Science, University of Saskatchewan, Saskatchewan, Canada, S7N5A8

6 ³ Department of Soil and Physical Sciences, Lincoln University, PO Box 85084, Lincoln, Christchurch,
7 New Zealand, 7647

8 ⁴ CSIRO Land and Water, Canberra, ACT, Australia, 2601

9 * Correspondence to: A. Biswas (asim.biswas@mcgill.ca Phone: +1 514 398 7620; Fax: +1 514 398
10 7990)

11

12 **Abstract** Spatio-temporal behavior of soil water is essential to understand the science of
13 hydrodynamics. Data intensive measurement of surface soil water using remote sensing has
14 established that the spatial variability of soil water can be described using the principle of self-
15 similarity (scaling properties) or fractal theory. This information can be used in determining land
16 management practices provided the surface scaling properties hold at deep layer. Current study
17 examined the scaling properties of sub-surface soil water and its relationship to surface soil water,
18 thereby serving as the supporting information for the plant root and vadose zone models. Soil water
19 storage (SWS) down to 1.4 m depth at seven equal intervals was measured along a transect of 576
20 m for 5 years. The surface SWS showed multifractal nature only during the wet period (from
21 snowmelt until mid to late June with large SWS) indicating the need of multiple scaling indices in
22 transferring soil water variability information over multiple scales. However, with increasing
23 depth, the SWS became monofractal in nature indicating the need of single scaling index to
24 upscale/downscale soil water variability information. The dynamic nature made the surface layer
25 soil water in the wet period highly variable compared to the deep layers. In contrast, all soil layers
26 during the dry period (from late June to the end of the growing season with low SWS) were
27 monofractal in nature, probably resulting from the high evapotranspirative demand of the growing
28 vegetation that surpassed other effects. This strong similarity between the scaling properties at the
29 surface layer and deep layers provides the possibility of inferring about the whole profile soil water
30 dynamics using the scaling properties of the easy-to-measure surface SWS data.

31 **Keywords** Scaling, scale invariance, monofractal, multifractal, root zone, remote sensing



32 **1 Introduction**

33 Knowledge on the spatial distribution of soil water over a range of spatial scales and time has
34 important hydrologic applications including assessment of land-atmosphere interactions
35 (Sivapalan, 1992), performance of various engineered covers, monitoring soil water balance and
36 validating various climatic and hydrological models (Rodriguez-Iturbe et al., 1995;Koster et al.,
37 2004). However, high variability in soil is a major challenge in hydrology (Quinn, 2004) as the
38 distribution of soil water in the landscape is controlled by various factors and processes operating
39 at different intensities over a variety of scales (Entin et al., 2000). The individual and/or combined
40 influence of these physical factors (e.g. topography, soil properties) and environmental processes
41 (e.g. runoff, evapotranspiration, and snowmelt) gives rise to complex and nested effects, which in
42 turn evolve a signature in the spatial organization (Western et al., 1999) or patterns in soil water
43 as a function of spatial scale (Kachanoski and Dejong, 1988;Kim and Barros, 2002;Biswas and Si,
44 2011a). This complexity makes the management decision difficult at a scale other than the scale
45 of measurement. Therefore, it is necessary to transfer variability information from one scale (e.g.
46 pedon scale) to another (e.g. large catchment scale), which is called scaling.

47 The scaling of soil water is possible if the distribution of some statistical parameters (e.g.,
48 variance) remain similar at all studied scales. This feature, known as scale-invariance, means that
49 the spatial feature in the distribution of soil water will not change if the length scales are multiplied
50 by a common factor (Hu et al., 1997). Generally, the soil water will have a typical size or scale, a
51 value around which individual measurements are centered. So the probability of measuring a
52 particular value will vary inversely as a power of that value, which is known as the power law
53 decay, a typical of scaling process. Now, as the spatial distribution of soil water follows the power
54 law decay (Hu et al., 1997;Kim and Barros, 2002;Mascaro et al., 2010), the spatial variability can
55 be investigated and characterized quantitatively over a large range of measurement scales using
56 fractal theory (Mandelbrot, 1982). When the spatial distribution of soil water is the response of
57 some linear processes, the scaling can be done using a single scaling coefficient over multiple
58 scales and the distribution shows monofractal scaling behaviour. However, the spatial distribution
59 of soil water is the nonlinear response of multiple factors and processes acting over a variety of
60 scales and therefore needs multiple scaling indices (multifractal scaling) in quantifying spatial
61 variability (Hu et al., 1997;Kim and Barros, 2002;Mascaro et al., 2010).



62 The multifractal scaling behaviour of soil water has been used in developing models to
63 downscale soil water estimate from remotely sensed measurements with a large foot print area.
64 The multifractal behaviour in the surface soil water as a result of temporal evolution of wetting
65 and drying has been reported from a sub-humid environment of Oklahoma by Kim and Barros
66 (2002). Mascaro et al. (2010) reported the multifractal behaviour of soil water, which was ascribed
67 as a signature of the rainfall spatial variability. Though these measurements can provide an
68 estimate of soil water over a large area quickly, they are limited to very few centimeters of the soil
69 profile. These studies reported the multifractal behaviour of only the surface soil water indicating
70 the superficial scaling properties. Surface soil layer is exposed to direct environmental forcing and
71 are most dynamic in nature. The scaling properties of surface soil water can be used for land
72 management practices provided the observed scaling properties holds for the deep layers such as
73 vadose zone or the whole soil profile. Understanding overall hydrological dynamics in soil profile
74 needs information on the scaling properties and the nature of the spatial variability of soil water
75 over a range of scales at deep layers as well (Biswas et al., 2012b). The information on the
76 similarity in the nature of the spatial variability of soil water between the surface layer and deep
77 layers may also help inferring about the soil profile hydrological dynamics. Therefore, the
78 objectives of this study were to examine the scaling properties of sub surface layers and their
79 relationship with surface layers at different initial soil water conditions over time. We have
80 examined the scaling properties of soil water storage at multiple depth layers and at soil layers
81 with increasing depth from the surface (cumulative depth) over a 5-year period from a hummocky
82 landscape from central Canada using the multifractal analysis. The relationship between the
83 scaling properties of the surface layer and the subsurface layers was also examined using the joint
84 multifractal analysis.

85 **2 Materials and Methods**

86 **2.1 Study site and data collection**

87 A field experiment was carried out at St. Denis National Wildlife Area (52°12'N lat. and 106°50'W
88 long.), which is located 40 km east of Saskatoon, Saskatchewan, Canada. The landscape of the
89 study area is hummocky with a complex sequence of slopes (10 to 15%) extending from different
90 sized rounded depressions to irregular complex knolls and knobs, a characteristic landscape of the
91 North American Prairie pothole region encompassing approximately 780,000 km² from north-



92 central United States to south-central Canada (National Wetlands Working Group, 1997). A
93 transect of 128 points (576 m long) extending in north-south direction was established in 2004 at
94 the study site to examine the soil water variation at field scale. The sample points were selected at
95 4.5 m regular interval along the transect to catch the systematic variability of soil water. Soil water
96 measurements were carried out at every 20 cm depth along the transect over the period of 2007 to
97 2011 and were used in this study to examine the fractal behavior of SWS at different depths of
98 over time. A detailed description of the study site, development of the transect, measurement of
99 soil water and the calibration of measurement instruments can be found in earlier publications from
100 this project (e.g. Biswas et al., 2012a).

101 **2.2 Data analysis**

102 Various methods including geostatistics, spectral analysis, and wavelet analysis have been used to
103 examine the scale-dependent spatial patterns of SWS. These methods generally deal with how the
104 second moment of SWS changes with scales or frequencies. When the statistical distribution of
105 SWS is normal, the second moment plus the average provide a complete description of the spatial
106 series. However, for other distributions (e.g. left skewed distribution), higher-order moments are
107 necessary for a complete description of the spatial series. For example, let's define the q^{th} moment
108 of a spatial series z as z^q . In this situation, for a positive value of q , the q^{th} moment magnify the
109 effect of larger numbers and diminish the effect of smaller numbers in z . While, on the other hand,
110 for a negative value of q , the q^{th} moment magnify the effect of small numbers and diminish the
111 effect of large numbers in the spatial series z . In this way, using variable moments, we can look at
112 the effect of the magnitude of the data in a series and characterize its spatial variability better.
113 There is a pressing need to summarize how these moments change with scales so that we can
114 compare and simulate spatially-variable SWS.

115 **2.2.1 Statistical self-similarity or scale invariance**

116 Soil water is highly variable in space and time. If the variability in the spatial/temporal distribution
117 remains statistically similar at all studied scales, the SWS is assumed to be self-similar (Evertsz
118 and Mandelbrot, 1992). Self-similarity, also called scale invariance, is closely associated with the
119 transfer of information from one scale to another (scaling). We used the multifractal analysis to
120 explore self-similarity or inherent differences in scaling properties of SWS in this study.

121



122 2.2.2 Multifractal analysis

123 On the spatial domain of the studied field, multifractal analysis was used to characterize the scaling
124 property of SWS by statistically measuring the mass distribution (Zelege and Si, 2004). The spatial
125 domain or the data along the transect was successively divided into self-similar segments following
126 the rule of the binomial multiplicative cascade (Evertsz and Mandelbrot, 1992). This method
127 required that the two segments divided from a unit interval to be of equal length. With regards to
128 a unit mass M (a normalized probability distribution of a variable or measured in a generalized
129 case) relating to the unit interval, the weight was also partitioned into $[h \times M]$ and $[(1-h) \times M]$,
130 where h was a random variable ($0 \leq h \leq 1$) governed by a probability density function. Sequentially,
131 the new subsets with its associated mass were equally divided into smaller parts. In this way,
132 multifractal analysis was able to describe the scaling properties for the higher-order moments
133 compared to semivariogram which can only measure the scaling properties of the second moment.
134 In a special case, if the scaling properties do not change with q , the spatial series can be identified
135 as monofractal, when one scaling coefficient is enough to characterize. Generally, the multifractal
136 analysis is good at measuring the highly fluctuated mass (box size) as well as providing physical
137 insights at all scales regardless of any ad hoc parameterization or homogeneity assumptions
138 (Schertzer and Lovejoy, 1987).

139 For SWS spatial series, the scale-invariant mass exponent, was termed as $\tau(q)$ (Liu and Molz
140 (1997):

$$141 \langle [\Delta z(x)]^q \rangle \propto x^{\tau(q)} \quad [1]$$

142 where z was the SWS spatial series, x was the lag distance and the symbol \propto indicated
143 proportionality. The $\tau(q)$ is widely used in multifractal analysis. If the plot of $\tau(q)$ vs. q [or $\tau(q)$
144 curve] has a single slope (i.e. a linear line), then the series is a simple scaling (monofractal) type.
145 If $\tau(q)$ curve is nonlinear and convex (facing downward), then the series is a multi-scaling
146 (multifractal) type. In this study, we used the UM model of Schertzer and Lovejoy (1987) to create
147 a linear reference line which represented the perfect monofractal type of scaling. Assuming the
148 conservation in mean value of SWS, this model simulated a cascade process with a scaling function
149 in an empirical moment. It is thus used here to compare and characterize the observed scaling
150 properties with a reference to the monofractal behavior. The goodness-of-fit between the $\tau(q)$
151 curves and the UM model was tested using the chi-square test. The sum of squared residuals



152 (SSRs) between the $\tau(q)$ curve and the UM model was also calculated to test the deviation. The
 153 $\tau(q)$ curves over the range of q values (in this study -15 to 15 at 0.5 interval) were fitted with a
 154 linear regression line (referred to as a single fit). The linear fitting of the $\tau(q)$ curves with $q < 0$ and
 155 $q > 0$ (referred to as segmented fit) were also completed. The difference between the mean of slopes
 156 and segmented fits (for positive and negative q values) was tested using the Student's t test.

157 With similar manner to Eq. [1], the q^{th} order normalized probability measure of SWS, $\mu(q, \varepsilon)$
 158 (also known as the partition function), is proved to vary with the scale size, as below

$$159 \quad \mu_i(q, \varepsilon) = \frac{[p_i(\varepsilon)]^q}{\sum_i [p_i(\varepsilon)]^q} \propto (\varepsilon/L)^{\tau(q)} \quad [2]$$

160 where ε is scale size in the i^{th} segment and $p_i(\varepsilon)$ is the probability of a measure and measures the
 161 concentration of a variable of interest (e.g. SWS) by dividing the value of the variable in the
 162 segment to the whole support length (e.g. to the whole transect of length L units) (Meneveau et al.,
 163 1990; Evertsz and Mandelbrot, 1992). The mass exponent $\tau(q)$ was related to the probability of
 164 mass distribution of SWS.

165 Moreover, the fractal dimension of the subsets of segments in scale size ε was measured by the
 166 multifractal spectrum $f(q)$. When a coarse Hölder exponent (local scaling indices) of α was in the
 167 limit as $\varepsilon \rightarrow 0$, $f(q)$ was calculated as below (Evertsz and Mandelbrot, 1992):

$$168 \quad f(q) = \lim_{\varepsilon \rightarrow 0} \left(\log \left(\frac{\varepsilon}{L} \right) \right)^{-1} \sum_i \mu_i(q, \varepsilon) \log \mu_i(q, \varepsilon) \quad [3]$$

169 and the local scaling indices, α , were given by

$$170 \quad \alpha(q) = \lim_{\varepsilon \rightarrow 0} \left(\log \left(\frac{\varepsilon}{L} \right) \right)^{-1} \sum_i \mu_i(q, \varepsilon) \log p_i(\varepsilon) \quad [4]$$

171 Noting that $f(\alpha)$ was determined through the Legendre transform of the $\tau(q)$ curve:
 172 $f(\alpha) = q\alpha(q) - \tau(q)$ (Chhabra and Jensen, 1989).

173 The multifractal spectrum is a powerful tool in portraying the similarity and/or differences
 174 between the scaling properties of the measures (e.g. SWS). This spectrum also enabled us to
 175 examine the local scaling property. The width of the spectrum ($\alpha_{\text{max}} - \alpha_{\text{min}}$) was used to examine



176 the heterogeneity in the local scaling indices. The wider the spectrum, the higher was the
177 heterogeneity in the distribution of SWS and vice versa. Similarly, the height of the spectrum
178 corresponded to the dimension of the scaling indices. The small $f(q)$ values indicated rare events
179 (extreme values in the distribution), whereas the largest value was the capacity dimension (D_0)
180 obtained at $q = 0$.

181 In addition to the multifractal spectrum, [$f(q)$ vs. $\alpha(q)$], for many practical applications, we
182 used models to incorporate a few selected indicators to describe the scaling property and variability
183 of a process. One of the widely used models for multifractal measure were the generalized
184 dimensions, which was calculated as below:

$$185 \quad D_q = \frac{1}{q-1} \lim_{\varepsilon \rightarrow 0} \frac{\log \sum_i P_i(\varepsilon)}{\log(\varepsilon)} \quad [5]$$

186 when $q = 1$, D_1 was referred to as the information dimension (also known as entropy dimension)
187 which provided information about the degree of heterogeneity in the measure distribution in
188 analogy to the entropy of an open system in thermodynamics (Voss, 1988). If the value of D_1 is
189 close to unity, it indicated the evenness of measures over the sets of cell size, while the value
190 approaching 0 indicated a subset of scale in which the irregularities were concentrated. The D_2 ,
191 known as the correlation dimension, was associated with the correlation function and measured
192 the average distribution density of the SWS (Grassberger and Procaccia, 1983). For a monofractal
193 distribution, the D_1 and D_2 tend to be equal to the D_0 . The same value of D_0 , D_1 and D_2 indicates
194 that the distribution exhibits perfect self-similarity and is homogeneous in nature. Contrarily, in
195 multifractal type scaling, the D_1 and D_2 tend to be smaller than D_0 , showing $D_0 > D_1 > D_2$.
196 Accordingly, the D_1/D_0 value can be used to describe the heterogeneity in the distribution
197 (Montero, 2005). The value equal to 1 indicated exact mono-scaling of the distribution.

198 **2.2.3 Joint multifractal analysis**

199 While the multifractal analysis characterized the distribution of a SWS spatial series along its
200 geometric support, the joint multifractal analysis was used to characterize the joint distribution of
201 two SWS spatial series along a common geometric support. As an extension of the multifractal
202 analysis, the length of the datasets was also divided into several segments in size ε . Two variables
203 ($P_i(\varepsilon)$ and $R_i(\varepsilon)$ representing two spatial series of SWS) were used here to measure the probability



204 of the measure in the i^{th} segment, when $P_i(\varepsilon) \propto (\varepsilon/L)^\alpha$ and $R_i(\varepsilon) \propto (\varepsilon/L)^\beta$. Among them, α and β
 205 were the local singularity strength which respectively represented the mean local exponents of
 206 $P_i(\varepsilon)$ and $R_i(\varepsilon)$ in the corresponding expressions above. The partition function for the joint
 207 distribution of $P_i(\varepsilon)$ and $R_i(\varepsilon)$, was calculated as below (Chhabra and Jensen, 1989; Meneveau et
 208 al., 1990; Zeleke and Si, 2004):

$$209 \quad \mu_i(q, t, \varepsilon) = \frac{p_i(\varepsilon)^q \cdot r_i(\varepsilon)^t}{\sum_{j=1}^{N(\varepsilon)} [p_j(\varepsilon)^q \cdot r_j(\varepsilon)^t]} \quad [6]$$

210 where the normalized μ is partition function, q and t were the real numbers for weighting. And the
 211 aforementioned local singularity strength (coarse Hölder exponents) α and β were the function to
 212 q and t as well:

$$213 \quad \alpha(q, t) = -[\ln(N(\varepsilon))]^{-1} \sum_{i=1}^{N(\varepsilon)} [\mu_i(q, t, \varepsilon) \cdot \ln(p_i(\varepsilon))] \quad [7]$$

$$214 \quad \beta(q, t) = -[\ln(N(\varepsilon))]^{-1} \sum_{i=1}^{N(\varepsilon)} [\mu_i(q, t, \varepsilon) \cdot \ln(r_i(\varepsilon))] \quad [8]$$

215 To indicate the dimension of the joint distribution, the multifractal spectra $f(\alpha, \beta)$, was given by

$$216 \quad f(\alpha, \beta) = -[\ln(N(\varepsilon))]^{-1} \sum_{i=1}^{N(\varepsilon)} [\mu_i(q, t, \varepsilon) \cdot \ln(\mu_i(q, t, \varepsilon))] \quad [9]$$

217 In fact, the joint partition function in Eq. [6] can be simplified to Eq. [2] when q or t is equal to 0.
 218 In this case, the joint multifractal spectrum was transformed to the multifractal spectrum with a
 219 single measure. When both value of q and t were 0, $f(\alpha, \beta)$ reached maximum and indicated box
 220 dimension of the geometric support of the measures. Pair value of α and β were determined by
 221 variable q and t . The Pearson correlation coefficient was used to quantitatively describe their
 222 relations across similar moment orders. In addition, correlation coefficients between the surface
 223 layer and subsurface layers were used as well to examine the similarity in the scaling properties.

224 **3 Results**

225 **3.1 Spatial pattern of soil water storage at different depths**



226 Average SWS for the surface 0-20 cm layer over five year period was 5.51 cm. A slight decrease
227 in SWS was observed at the immediate deep layer (20-40 cm) and a gradual increase thereafter.
228 Five-year average SWS was 5.45 cm, 5.48 cm, 5.56 cm, 5.61 cm, 5.69 cm and 5.77 cm for the 20-
229 40 cm, 40-60 cm, 60-80 cm, 80-100 cm, 100-120 cm and 120-140 cm layers, respectively (Table
230 1). Average SWS for a single measurement varied from 3.40 cm to 7.16 cm. The highest average
231 SWS was observed on 29 June 2011. The study area received large amount of spring rainfall during
232 2011 leading to the high SWS in the surface layer. The lowest average SWS was observed on 23
233 August 2008, which was one of the driest summer within the five-year study period. The highest
234 average SWS (on 29 June 2011) at the surface layer gradually decreased to 6.55 cm and the lowest
235 average SWS (on 23 August 2008) at the surface layer gradually increased to 5.28 cm at the 120-
236 140 cm layer (Table 1). This yielded a bigger range (3.76 cm) in the average SWS at the surface
237 layer compared to that at the deepest layer (1.27 cm). A big range (2.00 cm) in the standard
238 deviation (maximum=2.43 cm and minimum=0.43 cm) of the measurement at the surface layer (0-
239 20 cm) was also observed compared to that at the deepest layer (120-140 cm; maximum=1.28 and
240 minimum=0.76). This indicated large variations in SWS at the surface layer and gradually
241 decreased at deeper layers. The coefficient of variations (CVs) at the surface layer (0-20 cm) varied
242 from 10% to 43% and the deepest layer (120-140 cm) varied from 13% to 23% (Supplementary
243 Table S.1).

244 The maximum SWS at the surface layer also varied widely (maximum=13.96 cm and
245 minimum=4.64 cm) compared to the deepest layer (maximum=9.81 cm and minimum=6.72 cm)
246 (Table 1). There was a gradual decrease in the maximum value and increase in the minimum value
247 from the surface to the deepest layer. A similar trend was also observed for the minimum SWS at
248 different layers. The maximum SWS at different layers was much localized. For example, there
249 was high SWS at different layers at the locations of 100 to 140 m and 225 to 250 m from the origin
250 of the transect. These locations had very high SWS compared to the field-average and were situated
251 in the depressions while low SWS was observed on the knolls.

252 The variations in SWS with time were evaluated within a year. There was little change in the
253 average SWS over measurements within the years from 2007-2011 except 2008 (Table 1). For
254 example, average SWS was 6.47 cm, 6.03 cm, 6.54 cm, and 6.33 cm on 6 April 2010, 19 May
255 2010, 14 June 2010 and 28 September 2010, respectively. However, the average SWS in 2008
256 drops from 6.28 cm on 2 May 2008 to 3.51 cm on 17 September 2008 in the surface 0-20 cm layer.



257 This falling trend was even observed at all soil layers. When compared between years, the trend
258 over time and with depth was very similar in 2007 and 2009 while slightly different between 2010
259 and 2011 (Table 1). A decreasing trend of the variability was also observed with time. For example,
260 the CV of the surface layer was around 28% on 2 May 2008, which gradually decrease to around
261 13% on 17 September 2008 (Supplementary Table S.1).

262 The average water storage for soil layers with increasing depth was also calculated by adding
263 the individual layers together. The time-averaged values of SWS were 10.96 cm, 16.44 cm, 22.00
264 cm, 27.61 cm, 33.30 cm and 39.07 cm for the 0-40 cm, 0-60 cm, 0-80 cm, 0-100 cm, 0-120 cm
265 and 0-140 cm, respectively (Supplementary Table S.2). The CV of the 0-20 cm layer was the
266 highest during the wet period and gradually declined to the smallest during the dry period
267 (Supplementary Table S.3). The variability also gradually increased with depth. This trend with
268 depth and time has also been verified by the standard deviation of measurement.

269 **3.2 Statistical scale invariance**

270 The distribution of a statistical measure is considered as fractal (monofractal/multifractal) provided
271 the moments obey the power law (Evertsz and Mandelbrot, 1992). The power law relationships
272 and the statistical scale invariance were evaluated using a log-log plot of the aggregated variance
273 of SWS spatial series at different depths of soil layers and the level of disaggregation (or scales)
274 at different q values or statistical moments. The linear relationship of the logarithm of the variance
275 with scale indicated the presence of statistical scale invariance (Fig. 1). The scale invariance was
276 observed for all measurements and at all depths though only all depths of selected three
277 measurements were presented as example. The coefficient of determination (r^2) for a linear fit
278 ($n=7$) was between 0.99 and 1.00 (significant at $P=0.001$) for any measurement days and depths.
279 The scale invariance was also observed for SWS at soil layers with cumulative depths.

280 **3.3 Multifractal analysis**

281 The $\tau(q)$ curves for the surface layer displayed deviation from the UM model during the wet period
282 (Fig. 2). A high SSR value was observed between the $\tau(q)$ curves and the UM model. Nonlinearity
283 in the $\tau(q)$ curve was observed and the slopes of the segmented fit of the $\tau(q)$ curves were
284 significantly different from each other. For example, the SSR values between the $\tau(q)$ curve and
285 the UM model were 27.74 and 50.49 for the surface layer (0-20 cm) on 2 May 2008 and 31 May
286 2008, respectively. The slopes of the $\tau(q)$ curve for (single fit) were 0.97 and 0.96, respectively for



287 the surface layer of 2 May 2008 and 31 May 2008 (Fig. 2). The slopes of the segmented fit for
288 these measurements were 1.04 ($q < 0$) and 0.87 ($q > 0$) and, 1.06 ($q < 0$) and 0.82 ($q > 0$), respectively
289 (Fig. 2; Supplementary Table S.4).

290 With the maximum deviation at the surface layer, the $\tau(q)$ curves gradually became very similar
291 to the UM model with depth. The SSR value decreased considerably in the deep layers. The slopes
292 of the $\tau(q)$ curve (single fit) became almost unity with no significant difference with the UM model.
293 There was no significant difference between the slopes of the segmented fit. For example, the SSR
294 value was 6.17, 4.98, 8.80, 8.50, 8.86, and 6.16 respectively for the 20-40, 40-60, 60-80, 80-100,
295 100-120, and 120-140 cm layer of 2 May 2008 (Supplementary Table S.4). The slopes (single fit)
296 for these layers were 0.99, 1.00, 1.01, 1.01, 1.00, and 0.99, respectively (Fig. 2). The slopes of the
297 segmented fit were also very close to unity with no significant difference between them.

298 The SSR values gradually decreased and the slopes became almost unity with the increase of
299 depth of soil layers (Fig. 3). For example, the SSR values were 14.11, 9.31, 7.71, 6.86, 6.71 and
300 6.30 and the slopes (single fit) were 0.98, 0.99, 0.99, 1.00, 1.00, and 1.00, respectively for 0-40,
301 0-60, 0-80, 0-100, 0-120 and 0-140 cm layer (Supplementary Table S.5). The slopes of the
302 segmented fit for the $\tau(q)$ curve became almost the same as soil layers going deeper (Fig. 3). The
303 linearity of the $\tau(q)$ curves was gradually strengthened and the SSR value gradually fell with the
304 depth increase of soil layers at any time. A statically significant difference was observed between
305 the slopes of the $\tau(q)$ curves in segmented fitting at the surface layer of first three measurements
306 in 2007 (Supplementary Fig. S.1), two measurements in 2008 (Fig. 3), three measurements in 2009
307 (Supplementary Fig. S.2), and all measurements in 2010 and 2011 (Fig. 3).

308 A decreasing trend in the SSR value was also observed over time within a year. During the dry
309 period, the slopes (single fit and segmented fit) became almost unity with no significant difference
310 (Supplementary Table S.6). For example, the SSR value was 14.12, 8.25, 1.30, 1.46, and 0.52 and
311 the slope was 0.99, 0.99, 1.00, 1.00, and 1.00, respectively for the surface layer (0-20 cm) of 21
312 June 2008, 16 July 2008, 23 August 2008, 17 September 2008 and 22 October 2008 (Fig. 2).
313 Similarly, a small SSR value and consistent slope were also observed at the deepest layer (120-
314 140 cm). The SSR values of the 120-140 cm were 2.47, 2.47, 3.31, 3.44 and 4.57, respectively for
315 the measurements on 21 June 2008, 16 July 2008, 23 August 2008, 17 September 2008 and 22



316 October 2008 (Supplementary Table S.6). The slope (single fit) for all these measurements was
317 equal to 1.01 (Fig. 2). There was very little difference in the slopes of the segmented fits.

318 A significant difference in the slopes of the segmented fit was observed for the surface layer
319 (0-20 cm) of three measurements in 2007 (17 July, 7 August, and 1 September; Supplementary
320 Fig. S.1), and three measurements in 2009 (21 April, 7 May, and 27 May) (Supplementary Table
321 S.4; Supplementary Fig. S.2). The trend in deep layers over time was very similar to that of 2008.
322 However, the trend in the SSR values and the slopes with time was scarcely different between
323 2010 and 2011 (Supplementary Table S6). There was very little difference in the SSR values at
324 different time of the year. For example, the SSR value for the surface layer (0-20 cm) was 20.79,
325 27.18, 24.63 and 26.66 and the slope (single fit) was 0.97, 0.97, 0.97, and 0.97, respectively for
326 the measurements on 6 April 2010, 19 May 2010, 14 June 2010, and 28 September 2010 (Fig. 2).
327 The slope of the segmented fit of the surface layer (0-20 cm) was statistically significant for all
328 measurements in 2010 and 2011 (Fig. 2). However, the trend with depth was similar to other years
329 (Supplementary Table S.7).

330 The height of the multifractal spectrum at different depths of measurement over time was very
331 similar. The width of the spectrum ($\alpha_{\max}-\alpha_{\min}$) varied with depth and time. Generally, a comparative
332 large value of $\alpha_{\max}-\alpha_{\min}$ was observed at the surface layer during the wet period and the value
333 gradually became smaller at depths. For example, the value of $\alpha_{\max}-\alpha_{\min}$ for the surface soil layer
334 (0-20 cm) was 0.23 and 0.31, respectively for the measurements of 2 May 2008 and 31 May 2008.
335 Meanwhile, the value of $\alpha_{\max}-\alpha_{\min}$ for the soil layers of 20-140 cm with 20 cm increment was 0.15,
336 0.14, 0.19, 0.20, 0.20, and 0.18 for 2 May 2008 and 0.25, 0.19, 0.11, 0.14, 0.12, and 0.11 for 31
337 May 2008, respectively (Fig. 4). In the later part of the year, the width of the spectrum gradually
338 decreased (Supplementary Table S.8). For example, the $\alpha_{\max}-\alpha_{\min}$ values were 0.19, 0.16, 0.07,
339 0.08, and 0.05, respectively for the surface layer measurement of 21 June 2008, 16 July 2008, 23
340 August 2008, 17 September 2008 and 22 October 2008. Similar trend in values of $\alpha_{\max}-\alpha_{\min}$ was
341 also observed at deep layers (Fig. 4).

342 The trend of the $\alpha_{\max}-\alpha_{\min}$ values in 2007 and 2009 was very similar to that of 2008
343 (Supplementary Table S.8). A higher value of $\alpha_{\max}-\alpha_{\min}$ was observed in first three measurements
344 of 2007 (Supplementary Fig. S.5) and three measurements of 2009 (Supplementary Fig. S.6).
345 However, the values in the surface layer (0-20 cm) of measurements in 2010 and 2011 were always



346 higher compared to the deep layers (Fig. 4). There was no decreasing trend in values for the surface
347 layer over time. For example, the $\alpha_{\max}-\alpha_{\min}$ value was 0.21, 0.24, 0.21, and 0.22, respectively for
348 the measurements on 6 April 2010, 19 May 2010, 14 June 2010, and 28 September 2010 (Fig. 4).
349 However, the trend in the $\alpha_{\max}-\alpha_{\min}$ value of deep layers was similar to that of other years. A similar
350 trend was observed for cumulative SWS with increasing depth over the years (Fig. 5). Generally,
351 the value of $\alpha_{\max}-\alpha_{\min}$ was also small with the highest in the 0-20 soil layers and gradually
352 decreased with depth (Fig. 5; Supplementary Table S.9).

353 Generally, the D_1 and D_2 values for different depths of different measurements were very close
354 to 1 (only varied at 3 decimal points; Supplementary Table S.10). Specifically, the D values for
355 the surface layer during the wet period increased at high q values. For example, the first three
356 measurements in 2007 and 2009 all presented high D values at high q values (Supplementary Figs.
357 S.9 and S.10). This high D value gradually decreased in the dry period of the year. For example,
358 the D value with positive q was high in the surface layer of 2 May 2008 and 31 May 2008 (Fig.
359 6), whereas it gradually decreased at the later part of the year (e.g. 17 September 2008). The trend
360 with time and depth in 2007 and 2009 was very similar to that of 2008 (Supplementary Tables
361 S.10 and S.11). A consistent high D value was observed in the surface layer for all 2010 and 2011
362 measurements (Fig. 6). The trend in D values with depth in 2010 and 2011 was also similar to
363 other years. A high value of D_1 and D_2 were also observed at all layers of cumulative depths for
364 all measurements (Fig. 7; Supplementary Table S.11).

365 **3.4 Joint multifractal analysis**

366 There were strong correlations between the scaling property of the joint distribution of the surface
367 soil layer and the deep soil layers. The correlation between the surface 0-20 cm and the deep layers
368 on 2 May 2008 (wet period) was larger than 0.9 (significant at $P=0.001$; Table 2). The highest
369 correlation was observed between the layers closest to each other. The correlations gradually
370 increased over time and showed high consistency between different layers on 17 September 2008
371 (Table 2). A very similar trend was observed in other years.

372 **4 Discussion**

373 The amount of water stored in soil layers is the result of the dominant underlying hydrological
374 processes. Located in semi-arid climate, the study area receives about 30% of the long term annual
375 average precipitation as snowfall during winter months (Pomeroy et al., 2007). Generally, the



376 depressions receive snow from surrounding uplands or knolls as redistributed by strong prairie
377 wind (Pomeroy and Gray, 1995; Fang and Pomeroy, 2009). The snow melts within short period of
378 time during the early spring and contributed a large amount of water. The frozen ground restricts
379 infiltration and redistributes excess water within the landscape with greater accumulation in
380 depressions (Fig. 8) (Gray et al., 1985). Apart from the snowmelt, the spring rainfall also
381 contributes to the water inflow in the landscape (Fig. 8). This created a spatial pattern of SWS that
382 was almost a mirror image of the spatial distribution of relative elevation (Biswas and Si, 2011a,
383 b; Biswas et al., 2012a).

384 In the spring, the sources of water loss were the deep drainage and the evaporation. . As the
385 loss of water through deep drainage in the study area was as low as 2 to 40 mm per year, occurring
386 mainly through the fractures and preferential flow paths (Hayashi et al., 1998; van der Kamp et al.,
387 2003), the major loss occurred mainly through evaporation from the surface of the bare ground
388 and standing water in depressions. These processes lose a very small amount of water compared
389 to the input of the water in spring and early summer leaving the soil wet. Moreover, the surface
390 soil with high organic matter content and low bulk density stored larger amount of water than the
391 deep layers where the organic matter gradually decreased and the bulk density increased.
392 Reflecting the long-term history of vegetation growth in the landscape, the variability of organic
393 matter content (CV=41%) may be one of the main factor of the high variability in surface layer
394 SWS (Biswas and Si, 2011c)..

395 As the vegetation developed in summer, strong evapotranspiration resulted in the lowest
396 average SWS in a year. High amount of water in the depressions allowed grasses to grow faster
397 and transpire more water comparing to the knolls (Fig. 8). For example, the aquatic vegetation
398 growth within the depressions was as high as 2 m, while the grasses on the knolls grew to a
399 maximum up to a meter tall. The uneven growth of vegetation and the high evapotranspirative
400 demand in summer narrowed the range of SWS. Stronger demand extracted more water from the
401 soil where available and comparative less water from the soil where the availability was restricted,
402 thus reducing the disparities between maximum and minimum values. This variable water uptake
403 was visible in the growth of vegetation in the later part of the growing season as well (Fig. 8). The
404 reduction in the range of SWS was the largest in the surface layer and gradually decreased at deep
405 layers. This is because the surface layer was exposed to various environmental forcing and was
406 very dynamic in nature. For example, plants can take up more than 70% of the water they need



407 from the top 50% of the root zone (Feddes et al., 1978). This dynamic behavior of the surface layer
408 exhausted readily available water and finally reduced the range in water storage. This decrease in
409 range also happened in the later part of the growing season.

410 The multifractal and joint multifractal analyses explained the scaling behavior of SWS at
411 different depths over time. The linearity in the log-log plot between the aggregated variance in
412 SWS and the scale at all soil layers over time indicated the presence of scaling laws (Fig. 1). The
413 mass exponent, τ calculated over a range of moment orders (q) was used to examine the scaling
414 behavior (monofractal and multifractal). The shape of the curve described the type of scaling
415 involved. The curve with a single slope implied a monofractal scaling, while a convex downward
416 curve with different slopes for negative and positive moment orders implied a multiple scaling
417 (multifractal) (Evertsz and Mandelbrot, 1992). The deviation in the scaling property of SWS from
418 the monofractal was also examined by comparing the $\tau(q)$ curve with the theoretical UM model
419 and the SSR between them (Fig. 2). The near unity slope of the $\tau(q)$ curves and the insignificant
420 difference from the UM model indicated a monofractal type scaling at all layers except the surface
421 layer during the wet period (until mid to late June) where a multifractal behavior led to a slight
422 convex downward curve (Fig. 2). This was also supported by a significant difference between the
423 slope of single and segmented fit in the surface layer during the wet period.

424 Generally during the wet period, excess water fills and drains macropores quickly and creates
425 variations in SWS. Variations in the evaporation due to uneven solar incidence over micro-
426 topography also triggered SWS variability in the surface layer. Additionally, the snow melt and
427 the release of water controlled by local (e.g. soil texture) and non-local (e.g. topography) factors
428 also affected the spatial distribution of SWS, making it more heterogeneous in the wet period
429 (Grayson et al., 1997; Biswas and Si, 2012). Contrarily, as depth increased, less impact of
430 environmental forcing tended to create less variability in SWS and exhibited monofractal behavior
431 which was consistent with the uniform slope shown in Figure 2. During the dry period or later part
432 of the growing season, the SWS storage variability at all depths was small and exhibited
433 monofractal behavior (Fig. 2). Accordingly, the deeper layers in the wet period and all layers in
434 the dry period can be accurately represented by only one scaling exponent while the surface layer
435 in the wet period may require a hierarchy of exponents to describe scaling property. A similar trend
436 was observed in SWS of cumulative depth layers (Fig. 3). Resulting from increasingly buffering



437 capacity of the deeper soil layers, the variability of cumulative SWS overlaid the multifractal
438 nature of the surface layer, and finally exhibited monofractal behavior in general.

439 The scaling patterns of SWS at different depths and different periods were further examined
440 using multifractal spectrum [$f(q)$ vs. $\alpha(q)$] (Fig. 4 & Fig. 5). The degree of convexity was used to
441 characterize the heterogeneity of scaling exponents or the degree of multifractality. Large value of
442 $\alpha_{\max}-\alpha_{\min}$ indicated stronger heterogeneity in the local scaling indices of SWS or cumulative SWS
443 and vice versa. The largest value for the surface layer(s) in the wet period indicated the most
444 multifractal behavior of SWS. However, the value decreased with depth and gradually converged
445 in deep layers (Fig. 4). This decline manifested a conformity in the scaling behavior of SWS at
446 deeper layers. Over time, the $\alpha_{\max}-\alpha_{\min}$ value of the surface soil layer decreased and became very
447 similar to that of deep layers. This indicated a reduction in the degree of multifractality for surface
448 soil layers from the wet period to the dry period. A consistent $\alpha_{\max}-\alpha_{\min}$ value for all depths during
449 the dry period suggested the homogeneity and least multifractal nature of SWS. A similar behavior
450 was observed in the cumulative SWS (Fig. 5).

451 To sum up, both the unity slope of the $\tau(q)$ curves (Fig. 2 and Fig. 3) and the degree of
452 convexity of the $f(q)$ spectrum (Fig. 4 & Fig. 5) jointly demonstrated that dynamic behavior of
453 surface soil layers in the wet period made SWS highly variable and exhibited multifractal nature,
454 while less environmental forcing and increased buffering capacity of deep layers led to
455 monofractal nature. As a result, multiple scaling exponents were required to characterize the
456 variability of SWS in the surface layer during the wet period, while less number of exponents was
457 necessary for deeper layers during wet period or all layers during dry period.

458 The height of the spectrum, $f(q)$ revealed the dimension or frequency distribution of the scaling
459 indices. A low height of $f(q)$ curve indicated rare events or extreme values in the distribution, while
460 a high value represented uniform distribution in all segments. A very similar height of the $f(q)$
461 curve for all depths and all periods indicated a consistent frequency distribution of the scaling
462 indices. Additionally, the position and the symmetry of the curve revealed the distribution of
463 scaling exponents. A symmetric $f(q)$ curve indicated uniform distribution of the scaling exponents.
464 The left side of the spectrum corresponded to the large SWS that were amplified by the positive
465 values of q while the right side indicated smaller SWS that were amplified by negative q values.



466 Surface one or two layers during the wet period tended to exhibit longer tail of the curve on
467 the left, showing more heterogeneity in the distribution of large values. However, when stepping
468 into the dry period, the spectrum tended to display a longer tail on the right compared to the left
469 side, suggesting more heterogeneity in the distribution of smaller values. Few locations had
470 standing water thus large SWS during the wet period compared to few points with very small SWS
471 during the dry period owing to stronger demand by growing vegetation.

472 The generalized dimension, D_q was subsequently used to characterize the scaling property and
473 variability in SWS (Fig. 6 and Fig. 7). The largest value of $f(q)$, referred to as the capacity
474 dimension (D_0) obtained at $q = 0$, was close to unity for all layers at different times (Fig. 6). The
475 information dimension (D_1) obtained at $q = 1$ was different from correlation dimension (D_2), the
476 average distribution density of the measurement for the surface layers in the wet period
477 (Grassberger and Procaccia, 1983). In this case, the different values of D_0 , D_1 and D_2 indicated
478 multifractal nature of the distribution of SWS. Similarly, a non-unity value of D_1/D_0 (Montero,
479 2005) also indicated multifractal nature of SWS at the surface layer(s) during the wet period.
480 However, over the growing season, the D_1 and D_2 value approached closer to D_0 and indicated
481 monofractal type behavior. Similar values of D_0 , D_1 and D_2 during the dry period also indicated
482 homogeneous distribution.

483 Joint multifractal distribution between the surface and various subsurface layers indicated the
484 similarity in the scaling patterns (Table 2). Basically, the hydrological processes of shallower
485 layers was more similar to the top layer, while deeper layers showed more observable disparities
486 from the surface. The nearest subsurface (20-40 cm) layer showed generally the highest similarity
487 with the surface (0-20 cm) layer. However, in the wet period, the subsurface layers displayed the
488 smallest similarity to the surface layer, suggesting higher dynamic nature of hydrological
489 processes. In the dry period, stronger effect of vegetation overwhelmed the effect of small
490 variations, thus creating a more uniform distribution of SWS at all soil layers and showed stronger
491 similarity to the surface layers (Table 2).

492 Overall, our result revealed multifractal behavior of surface soil layers during the wet period
493 due to its dynamic nature. This behavior gradually changed with depth and time (Fig. 9). In the
494 deeper layers during the wet period, the behavior became less multifractal or nearly monofractal.
495 Similarly, in the dry period, the vegetation development and its high evapotranspirative demand



496 in semi-arid climate of the study area increasingly buffered the variation of SWS, as a result, all
497 the soil layers with less effect from environment forcing showed uniform distribution or
498 monofractal behavior (Fig. 9).

499 **5 Summary and Conclusions**

500 The transformation of information on soil water variability from one scale to another requires
501 knowledge on the scaling behaviour and the quantification of scaling index. Surface soil water can
502 be easily measured (e.g. remote sensing) and presents multi-scaling behaviour (requiring multiple
503 scaling indices). However, land-management practices requires the understanding of the
504 hydrological dynamics in the root zone and/or the whole soil profile. The scaling properties of the
505 surface soil layer can be used in the decision making provided the similar behavior holds at the
506 deep soil layer.

507 In this manuscript, the scaling properties of soil water storage at different soil layers measured
508 over five-year period were examined using multifractal and joint multifractal analysis. The scaling
509 properties of soil water storage mainly suggested monofractal scaling behavior. However, the
510 surface layer in the wet period or with high soil water storage tended to be multifractal in nature,
511 which gradually became monofractal with depth. With the decrease in soil water storage, the
512 scaling behavior became monofractal in nature at the later part of the year or growing season. The
513 year with high annual precipitation stored more water in the surface layer throughout the growing
514 period and displayed nearly multifractal scaling behavior. This multifractal nature indicated that
515 the transformation of information from one scale to another at the surface layer during the wet
516 period requires multiple scaling indices. On the contrary, the transformation requires single scaling
517 index during the dry period for the whole soil profile. The scaling properties of the surface layer
518 were highly correlated with that of the deep layers, which indicated a highly similar scaling
519 behaviour in the soil profile. The study was conducted in an undulating landscape from a semi-
520 arid climate and the results were very persistence over the years. Therefore, the observation
521 completed at the field scale in this type of landscape and climate may be generalized in similar
522 landscapes and climatic situations, otherwise may need to be examined thoroughly. The method
523 used here can be transferred to examine the scaling properties in other experimental situations.

524 **6 Acknowledgements**



525 The project was funded by the Natural Science and Engineering Research Council of Canada. The
526 help from the graduate student and the summer students of the Department of Soil Science at the
527 University of Saskatchewan in collecting field data is highly appreciated.

528 **7 References**

- 529 Biswas, A., and Si, B. C.: Scales and locations of time stability of soil water storage in a hummocky
530 landscape, *J. Hydrol.*, 408, 100-112, 10.1016/j.jhydrol.2011.07.027, 2011a.
- 531 Biswas, A., and Si, B. C.: Revealing the Controls of Soil Water Storage at Different Scales in a
532 Hummocky Landscape, *Soil Sci. Soc. Am. J.*, 75, 1295-1306, 10.2136/sssaj2010.0131, 2011b.
- 533 Biswas, A., and Si, B. C.: Identifying scale specific controls of soil water storage in a hummocky
534 landscape using wavelet coherency, *Geoderma*, 165, 50-59, 10.1016/j.geoderma.2011.07.002,
535 2011c.
- 536 Biswas, A., Chau, H. W., Bedard-Haughn, A. K., and Si, B. C.: Factors controlling soil water
537 storage in the hummocky landscape of the Prairie Pothole Region of North America, *Can. J.*
538 *Soil Sci.*, 92, 649-663, 10.4141/cjss2011-045, 2012a.
- 539 Biswas, A., and Si, B. C.: Identifying effects of local and nonlocal factors of soil water storage
540 using cyclical correlation analysis, *Hydrol. Proc.*, 26, 3669-3677, 10.1002/hyp.8459, 2012.
- 541 Biswas, A., Zeleke, T. B., and Si, B. C.: Multifractal detrended fluctuation analysis in examining
542 scaling properties of the spatial patterns of soil water storage, *Nonlin. Proc. Geophys.*, 19, 227-
543 238, 10.5194/npg-19-227-2012, 2012b.
- 544 Chhabra, A., and Jensen, R. V.: Direct determination of the $f(\alpha)$ singularity spectrum, *Physical*
545 *Review Letters*, 62, 1327-1330, 1989.
- 546 Entin, J. K., Robock, A., Vinnikov, K. Y., Hollinger, S. E., Liu, S. X., and Namkhai, A.: Temporal
547 and spatial scales of observed soil moisture variations in the extratropics, *J. Geophys. Res.-*
548 *Atm.*, 105, 11865-11877, 10.1029/2000jd900051, 2000.
- 549 Evertsz, C. J. G., and Mandelbrot, B. B.: Self-similarity of harmonic measure on DLA, *Physica A:*
550 *Statistical Mechanics and its Applications*, 185, 77-86, [http://dx.doi.org/10.1016/0378-](http://dx.doi.org/10.1016/0378-4371(92)90440-2)
551 [4371\(92\)90440-2](http://dx.doi.org/10.1016/0378-4371(92)90440-2), 1992.
- 552 Fang, X., and Pomeroy, J. W.: Modelling blowing snow redistribution to prairie wetlands, *Hydrol.*
553 *Proc.*, 23, 2557-2569, 10.1002/hyp.7348, 2009.
- 554 Feddes, R. A., Kowalik, P. J., and Zaradny, H.: Simulation of field water use and crop yield., John
555 Wiley & Sons Inc., New York, 1978.
- 556 Grassberger, P., and Procaccia, I.: Characterization of Strange Attractors, *Physical Review Letters*,
557 50, 346-349, 1983.
- 558 Gray, D. M., Landine, P. G., and Granger, R. J.: SIMULATING INFILTRATION INTO FROZEN
559 PRAIRIE SOILS IN STREAMFLOW MODELS, *Can. J. Earth Sci.*, 22, 464-472, 1985.
- 560 Grayson, R. B., Western, A. W., Chiew, F. H. S., and Blöschl, G.: Preferred states in spatial soil
561 moisture patterns: Local and nonlocal controls, *Water Resour. Res.*, 33, 2897-2908, 1997.
- 562 Hayashi, M., van der Kamp, G., and Rudolph, D. L.: Water and solute transfer between a prairie
563 wetland and adjacent uplands, 2. Chloride cycle, *J. Hydrol.*, 207, 56-67, 1998.
- 564 Hu, Z. L., Islam, S., and Cheng, Y. Z.: Statistical characterization of remotely sensed soil moisture
565 images, *Remote Sensing of Environment*, 61, 310-318, 1997.
- 566 Kachanoski, R. G., and Dejong, E.: Scale dependence and the temporal persistence of spatial
567 patterns of soil-water storage, *Water Resour. Res.*, 24, 85-91, 1988.



- 568 Kim, G., and Barros, A. P.: Downscaling of remotely sensed soil moisture with a modified fractal
 569 interpolation method using contraction mapping and ancillary data, *Remote Sensing of*
 570 *Environment*, 83, 400-413, 2002.
- 571 Koster, R. D., Dirmeyer, P. A., Guo, Z. C., Bonan, G., Chan, E., Cox, P., Gordon, C. T., Kanae,
 572 S., Kowalczyk, E., Lawrence, D., Liu, P., Lu, C. H., Malyshev, S., McAvaney, B., Mitchell,
 573 K., Mocko, D., Oki, T., Oleson, K., Pitman, A., Sud, Y. C., Taylor, C. M., Verseghy, D., Vasic,
 574 R., Xue, Y. K., Yamada, T., and Team, G.: Regions of strong coupling between soil moisture
 575 and precipitation, *Science*, 305, 1138-1140, 10.1126/science.1100217, 2004.
- 576 Liu, H. H., and Molz, F. J.: Multifractal analyses of hydraulic conductivity distributions, *Water*
 577 *Resour. Res.*, 33, 2483-2488, 10.1029/97WR02188, 1997.
- 578 Mandelbrot, B. B.: *The fractal geometry of nature*, W.H. Freeman and Company, San Francisco,
 579 1982.
- 580 Mascaro, G., Vivoni, E. R., and Deidda, R.: Downscaling soil moisture in the southern Great Plains
 581 through a calibrated multifractal model for land surface modeling applications, *Water Resour.*
 582 *Res.*, 46, W08546, 10.1029/2009WR008855, 2010.
- 583 Meneveau, C., Sreenivasan, K. R., Kailasnath, P., and Fan, M. S.: Joint multifractal measures:
 584 Theory and applications to turbulence, *Physical Review A*, 41, 894-913, 1990.
- 585 Montero, E. s.: Rényi dimensions analysis of soil particle-size distributions, *Ecological Modelling*,
 586 182, 305-315, <http://dx.doi.org/10.1016/j.ecolmodel.2004.04.007>, 2005.
- 587 National Wetlands Working Group: *The Canadian wetland classification system*, University of
 588 Waterloo, ON, 1997.
- 589 Pomeroy, J. W., and Gray, D. M.: Snowcover, accumulation, relocation, and management, in:
 590 NHRI Science Report No. 7, Environment Canada, Saskatoon, SK., 144, 1995.
- 591 Pomeroy, J. W., de Boer, D., and Martz, L. W.: Hydrology and water resources, in: *Saskatchewan:*
 592 *Geographic Perspectives*, edited by: Thraves, B., CRRC, Regina, SK, Canada, 2007.
- 593 Quinn, P.: Scale appropriate modelling: representing cause-and-effect relationships in nitrate
 594 pollution at the catchment scale for the purpose of catchment scale planning, *J. Hydrol.*, 291,
 595 197-217, 10.1016/j.hydrol.2003.12.040, 2004.
- 596 Rodriguez-Iturbe, I., Vogel, G. K., Rigon, R., Entekhabi, D., Castelli, F., and Rinaldo, A.: ON
 597 THE SPATIAL-ORGANIZATION OF SOIL-MOISTURE FIELDS, *Geophys. Res. Lett.*, 22,
 598 2757-2760, 10.1029/95gl02779, 1995.
- 599 Schertzer, D., and Lovejoy, S.: Physical modeling and analysis of rain and clouds by anisotropic
 600 scaling multiplicative processes, *Journal of Geophysical Research: Atmospheres*, 92, 9693-
 601 9714, 10.1029/JD092iD08p09693, 1987.
- 602 Sivapalan, M.: Scaling of hydrologic parameterizations, 1. Simple models for the scaling of
 603 hydrologic state variables, examples and a case study, Center for Water Research, University
 604 of Western Australia, Nedlands, WA, Australia, 1992.
- 605 van der Kamp, G., Hayashi, M., and Gallen, D.: Comparing the hydrology of grassed and
 606 cultivated catchments in the semi-arid Canadian prairies, *Hydrol. Proc.*, 17, 559-575,
 607 10.1002/hyp.1157, 2003.
- 608 Voss, R.: Fractals in nature: From characterization to simulation, in: *The Science of Fractal*
 609 *Images*, edited by: Peitgen, H.-O., and Saupe, D., Springer New York, 21-70, 1988.
- 610 Western, A. W., Grayson, R. B., Bloschl, G., Willgoose, G. R., and McMahon, T. A.: Observed
 611 spatial organization of soil moisture and its relation to terrain indices, *Water Resour. Res.*, 35,
 612 797-810, 1999.



613 Zeleke, T. B., and Si, B. C.: Scaling properties of topographic indices and crop yield: Multifractal
614 and joint multifractal approaches, *Agron. J.*, 96, 1082-1090, 2004.

615

616 **Figure captions**

617 Fig. 1. Log-log plot between the aggregated variance of the SWS spatial series and the scale. A
618 linear relationship indicated the presence of scale invariance and scaling laws.

619 Fig. 2. Mass exponents for soil water storage spatial series measured at each 20 cm soil layer down
620 to 140 cm in 2008 and 2010 for a range of q (-15 to 15 at 0.5 increments). The solid line is a linear
621 reference created following the UM model of Schertzer and Lovejoy (1987) passing through ($q =$
622 0).

623 Fig. 3. Mass exponents for soil water storage spatial series from surface to different soil layers
624 (cumulative storage) at 20 cm increment down to 140 cm in 2008 and 2010 for a range of q (-15
625 to 15 at 0.5 increments). The solid line is a linear reference created following the UM model of
626 Schertzer and Lovejoy (1987) passing through ($q = 0$).

627 Fig. 4. Multifractal spectra of soil water storage spatial series measured at each 20 cm soil layer
628 down to 140 cm in 2008 and 2010 for a range of q (-15 to 15 at 0.5 increments).

629 Fig. 5. Multifractal spectra of soil water storage spatial series from surface to different soil layers
630 (cumulative storage) at 20 cm increment down to 140 cm in 2008 and 2010 for a range of q (-15
631 to 15 at 0.5 increments).

632 Fig. 6. Generalized dimension spectra of soil water storage spatial series measured at each 20 cm
633 soil layer down to 140 cm in 2008 and 2010 for a range of q (-15 to 15 at 0.5 increments).

634 Fig. 7. Generalized dimension spectra of soil water storage spatial series from surface to different
635 soil layers (cumulative storage) at 20 cm increment down to 140 cm in 2008 and 2010 for a range
636 of q (-15 to 15 at 0.5 increments).

637 Fig. 8: Conceptual schematics showing the vegetation growth patterns in the different section of
638 landscapes at different times of the year. The figure is developed based on field observations and
639 the scale is arbitrary.

640 Fig. 9: Conceptual schematics showing vegetation development over time, dominant water loss
641 processes and the scaling behavior of soil water storage at different depths. The figure is developed
642 based on field observations and scaling analysis. The scale of the figure is arbitrary.



643 **Tables**

644 Table 1. Maximum, minimum, and average soil water storage at different depths (20 cm increment) over the whole measurement period.

	0-20 cm			20-40 cm			40-60 cm			60-80 cm			80-100 cm			100-120 cm			120-140 cm		
	Maximum (cm)	Minimum (cm)	Average (cm)	Maximum (cm)	Minimum (cm)	Average (cm)	Maximum (cm)	Minimum (cm)	Average (cm)	Maximum (cm)	Minimum (cm)	Average (cm)	Maximum (cm)	Minimum (cm)	Average (cm)	Maximum (cm)	Minimum (cm)	Average (cm)	Maximum (cm)	Minimum (cm)	Average (cm)
Jul 17 2007	13.96	3.25	5.65	11.55	3.09	5.63	9.43	2.59	5.73	9.06	3.34	5.90	9.51	3.22	5.89	9.81	3.55	6.05	9.81	3.54	6.14
Aug 7 2007	13.96	3.05	4.90	9.28	2.73	5.04	8.30	2.40	5.21	9.36	2.75	5.48	8.23	2.96	5.57	7.52	3.17	5.62	9.11	3.17	5.67
Sept 1 2007	13.96	2.26	5.29	9.28	3.00	5.08	8.08	2.42	5.23	6.98	2.75	5.38	7.17	2.92	5.52	8.08	3.20	5.64	9.07	3.23	5.73
Oct 12 2007	8.30	3.40	5.04	6.92	3.07	5.03	6.74	2.43	5.19	7.60	2.81	5.36	8.39	2.93	5.48	7.92	3.25	5.60	8.55	3.25	5.67
May 2 2008	13.96	4.49	6.28	9.96	4.09	6.03	9.43	3.69	5.80	8.83	3.16	5.74	9.51	2.90	5.66	9.81	3.26	5.70	9.81	3.30	5.75
May 31 2008	13.96	3.30	5.21	9.28	1.54	5.51	8.08	1.58	5.55	6.85	3.00	5.58	7.08	3.08	5.64	8.08	3.22	5.70	8.39	3.25	5.79
Jun 21 2008	8.77	3.06	4.70	7.84	3.43	5.25	6.86	2.80	5.38	6.78	2.77	5.52	7.08	3.04	5.61	7.73	3.28	5.69	8.48	3.23	5.77
July 16 2008	7.07	2.78	4.03	6.78	3.06	4.77	6.71	2.60	5.10	6.75	2.56	5.30	6.84	2.91	5.43	6.98	3.17	5.56	7.01	3.16	5.64
Aug 23 2008	4.96	2.44	3.40	5.66	2.73	4.11	6.02	2.37	4.59	6.44	2.36	4.90	6.56	2.63	5.12	6.85	3.04	5.30	6.81	2.99	5.42
Sept 17 2008	4.64	2.66	3.51	5.63	2.79	4.07	5.91	2.49	4.55	6.28	2.45	4.85	6.59	2.63	5.05	6.68	3.05	5.25	6.91	2.96	5.37
Oct 22 2008	6.11	3.83	4.96	6.03	3.10	4.37	5.92	2.52	4.53	6.13	2.46	4.79	6.55	2.63	5.00	6.61	3.00	5.18	6.73	1.22	5.28
April 20 2009	13.96	4.73	6.67	11.55	3.62	5.84	10.49	3.23	5.62	8.83	2.97	5.48	9.51	2.67	5.38	9.81	3.08	5.49	9.81	2.85	5.66
May 7 2009	13.96	4.45	5.97	9.51	3.68	5.70	8.08	3.26	5.49	8.30	3.00	5.36	7.85	2.73	5.35	9.81	3.01	5.43	8.91	2.84	5.51
May 27 2009	12.60	3.67	5.43	8.15	3.55	5.52	8.08	3.43	5.39	6.78	3.13	5.37	7.16	2.64	5.39	8.08	2.96	5.51	8.45	2.80	5.53
July 21 2009	6.92	3.16	4.56	7.24	3.16	4.83	6.55	2.91	5.00	6.72	2.95	5.23	6.77	2.58	5.24	6.91	3.02	5.34	6.89	3.24	5.43
Aug 27 2009	6.64	3.42	5.01	6.67	3.57	5.07	6.32	2.84	4.92	6.50	2.85	5.03	6.76	2.57	5.16	6.79	3.00	5.25	6.90	3.02	5.34
Oct 27 2009	6.65	3.89	5.30	6.44	3.44	4.90	6.04	2.74	4.80	6.36	2.68	4.91	6.55	2.60	5.05	6.71	3.05	5.17	6.71	2.79	5.29
April 6 2010	13.96	4.67	6.47	9.51	3.53	5.52	9.43	3.19	5.31	8.83	2.91	5.35	9.51	2.61	5.23	9.81	3.01	5.34	9.81	2.83	5.41
May 19 2010	13.96	4.08	6.04	11.32	4.28	5.94	10.49	4.46	5.94	8.75	4.08	5.93	8.60	3.55	5.90	9.81	4.03	5.91	9.81	3.96	5.85
June 14 2010	13.96	4.38	6.54	11.55	4.48	6.32	10.49	4.58	6.31	8.83	4.27	6.29	9.51	3.86	6.22	9.81	4.37	6.24	9.81	4.50	6.20
Sept 28, 2010	13.96	4.51	6.33	11.55	4.48	6.16	9.43	3.77	6.08	8.83	3.91	6.13	9.51	3.83	6.12	9.81	4.11	6.16	9.79	4.18	6.20
May 13, 2011	13.96	4.82	7.12	11.55	4.87	6.61	10.49	4.75	6.50	9.21	4.54	6.40	9.51	4.16	6.34	9.96	3.17	6.32	9.79	4.30	6.45
Jun 6, 2011	13.96	4.31	7.05	11.55	4.56	6.59	10.49	3.85	6.52	9.06	4.75	6.44	9.51	4.21	6.40	9.96	3.17	6.39	9.79	4.77	6.52
Jun 29, 2011	13.96	4.93	7.16	11.55	4.96	6.73	10.49	4.29	6.64	9.74	4.42	6.57	9.51	4.28	6.49	9.96	3.17	6.46	9.79	4.30	6.55
Sept 29, 2011	12.60	3.11	5.25	8.15	3.46	5.50	8.08	2.88	5.68	7.58	4.03	5.82	9.19	3.77	5.89	9.51	3.81	6.02	9.36	4.14	6.04

645



646 Table 2: Correlation between joint multifractal coefficients of surface to different subsurface
 647 layers measured at 20 cm interval in 2008.

	2 May 2008	31 May 2008	21 Jun. 2008	16 Jul. 2008	23 Aug. 2008	17 Sep. 2008	22 Oct. 2008
0-20 cm vs. 20-40 cm	0.96	0.98	0.99	0.99	0.99	1.00	1.00
0-20 cm vs. 40-60 cm	0.93	0.96	0.96	0.97	0.97	1.00	1.00
0-20 cm vs. 60-80 cm	0.93	0.94	0.95	0.95	0.96	0.99	0.99
0-20 cm vs. 80-100 cm	0.92	0.92	0.93	0.94	0.94	0.98	0.99
0-20 cm vs. 100-120 cm	0.92	0.92	0.93	0.93	0.93	0.97	0.99
0-20 cm vs. 120-140 cm	0.93	0.94	0.95	0.94	0.94	1.00	1.00

648

649

650

651

652

653

654

655

656

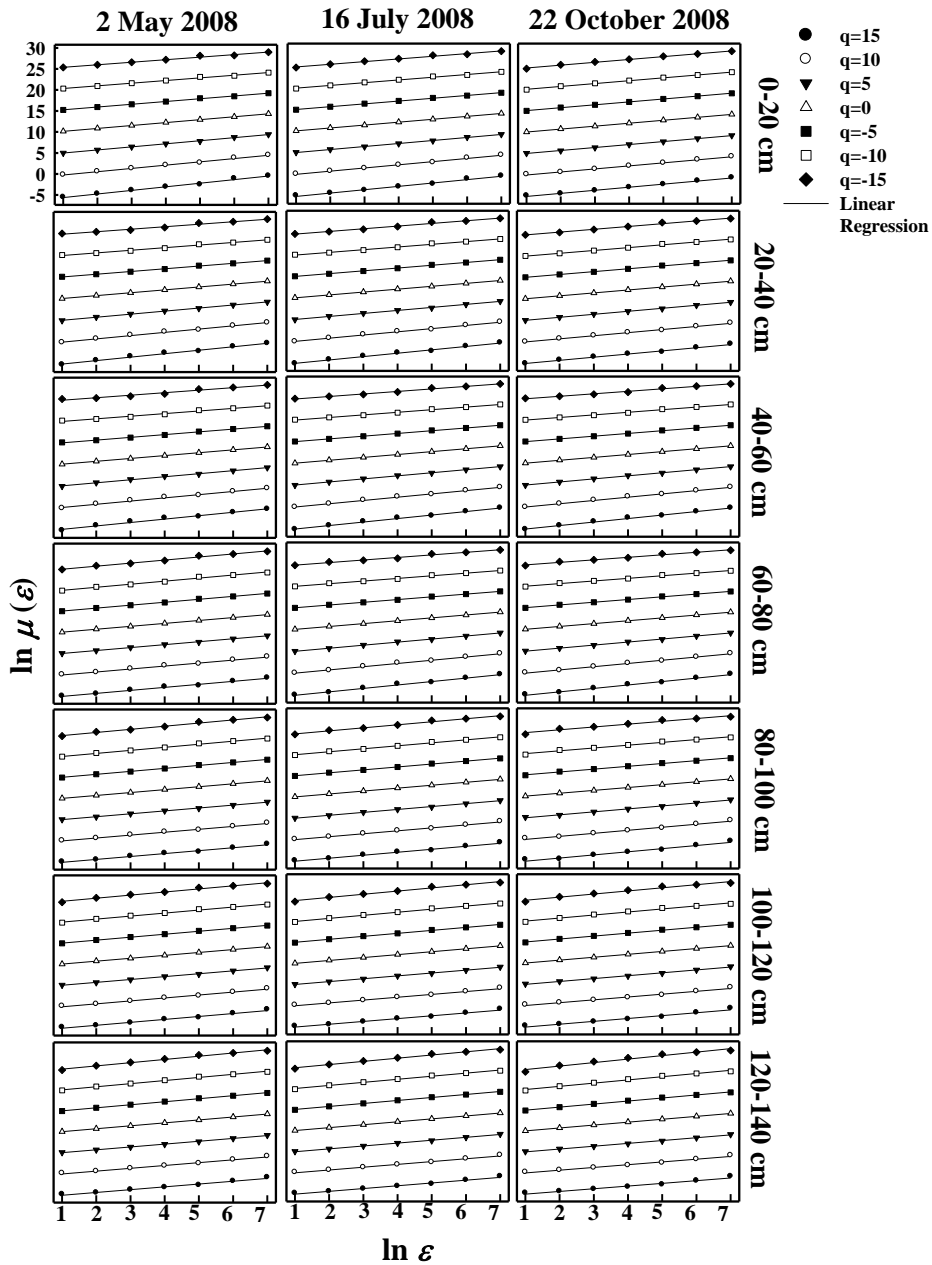
657

658

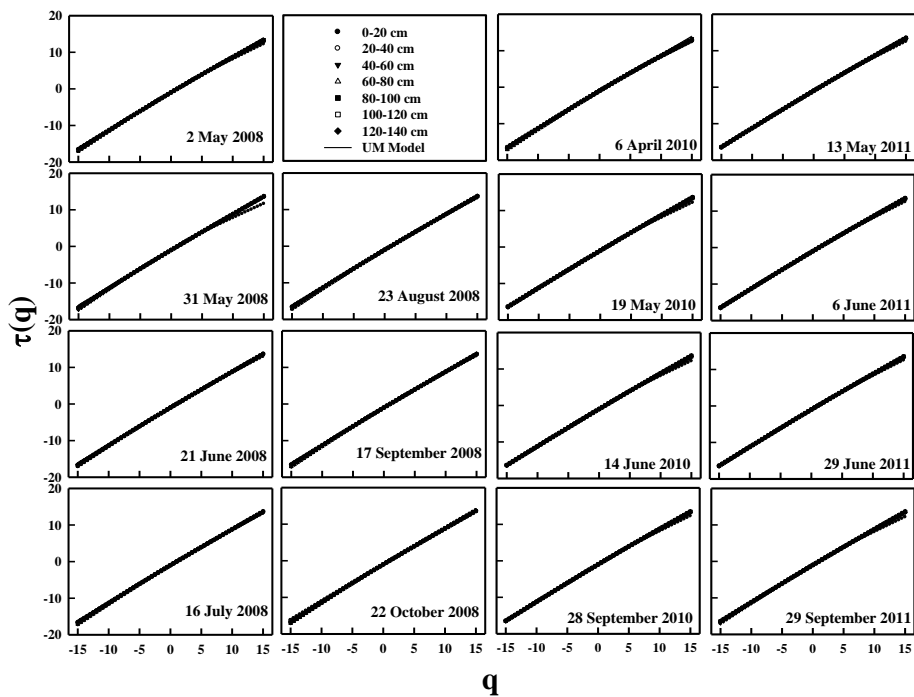
659



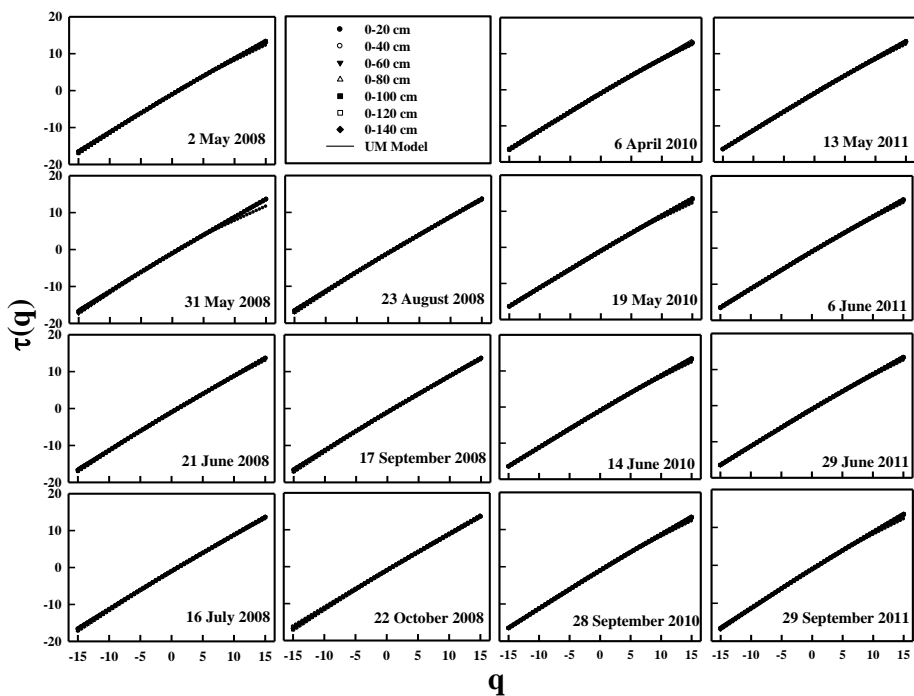
660 **Figures**



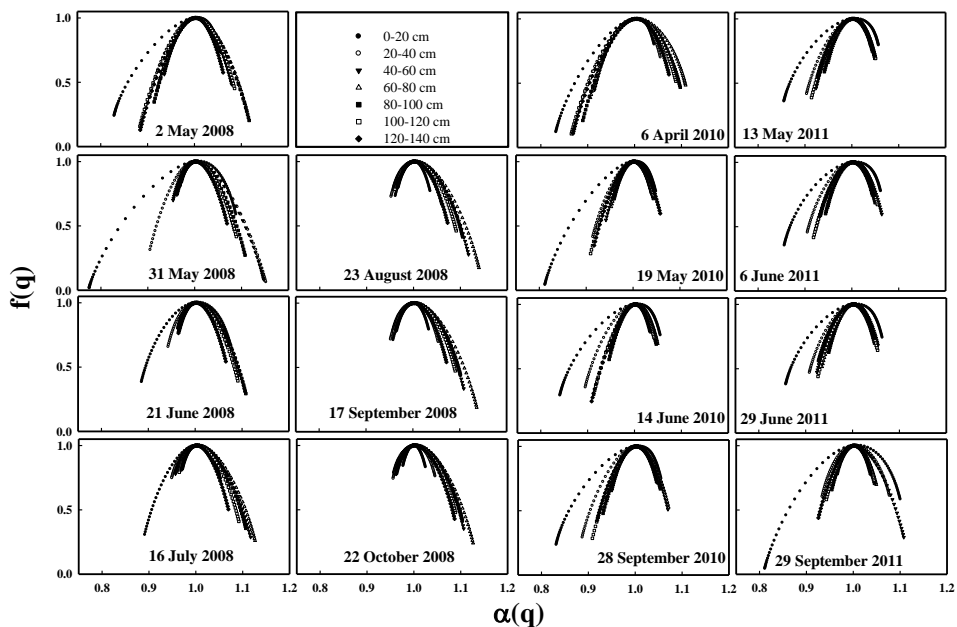
661
 662 **Figure 1**



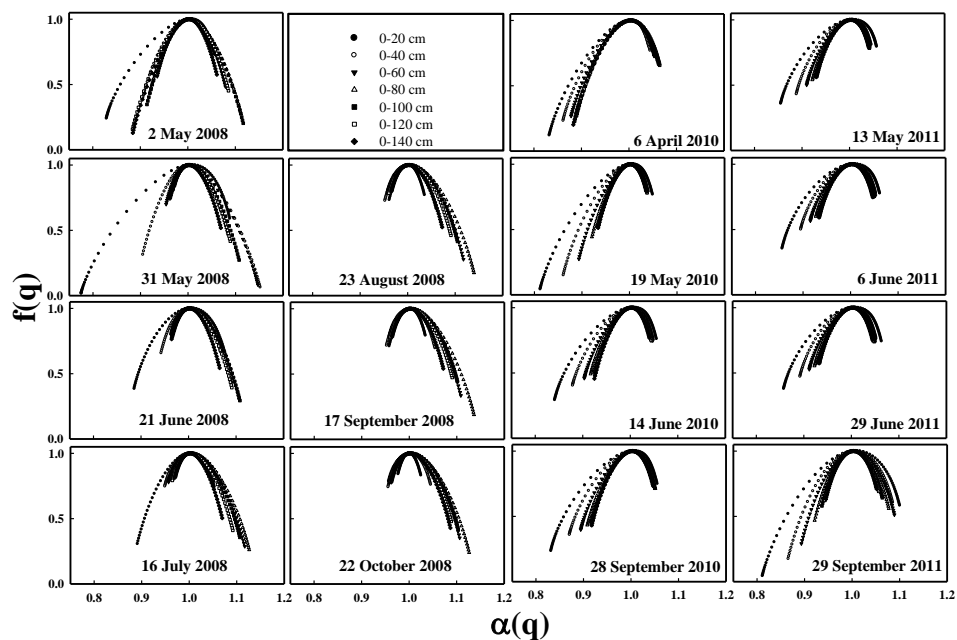
663
 664 Figure 2



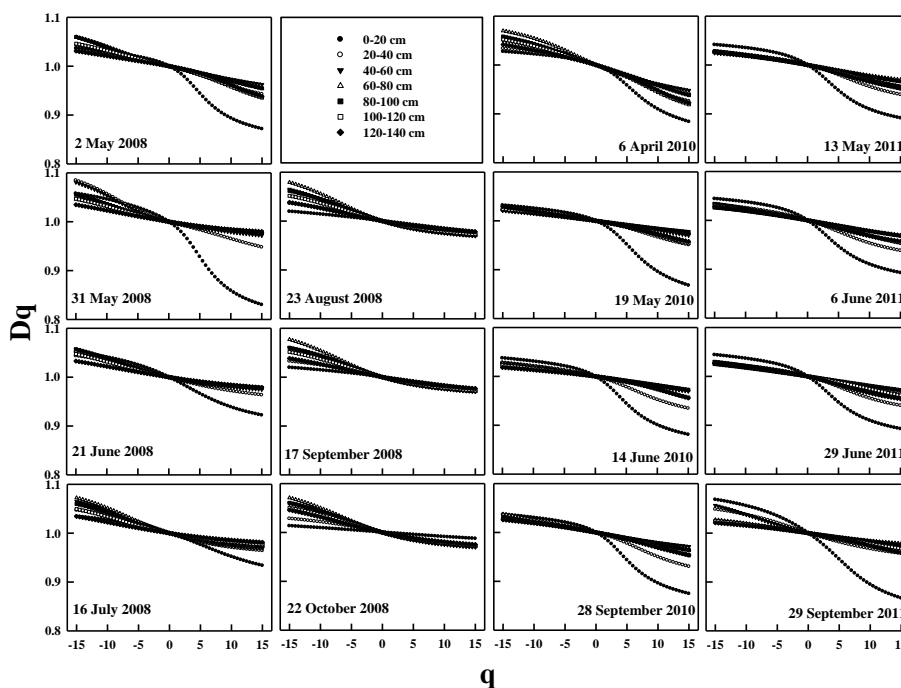
665
 666 Figure 3



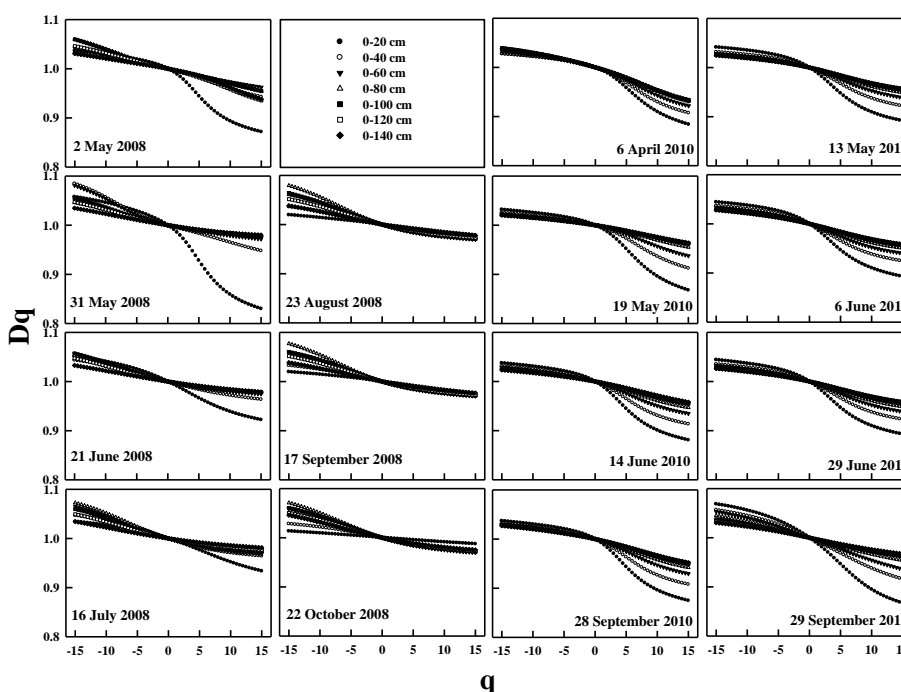
667
 668 Figure 4



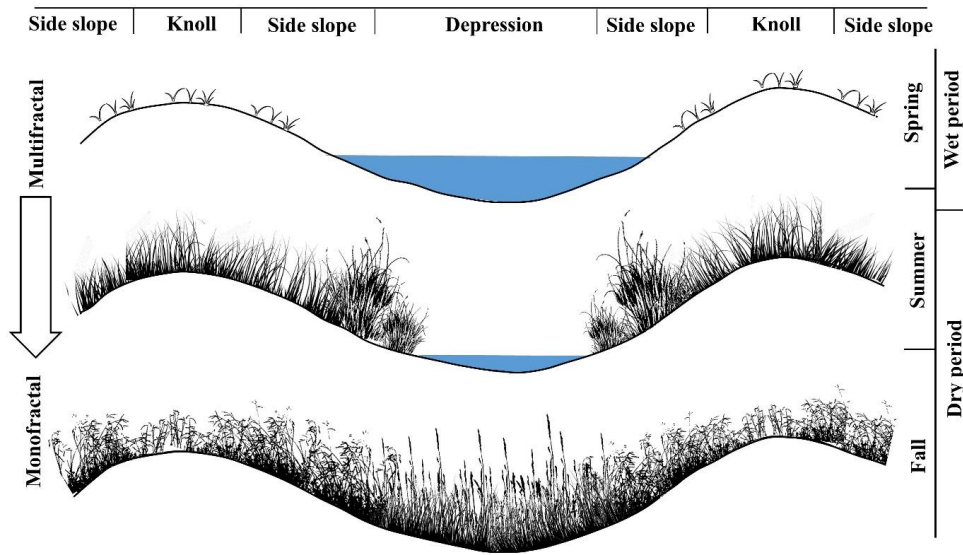
669
 670 Figure 5



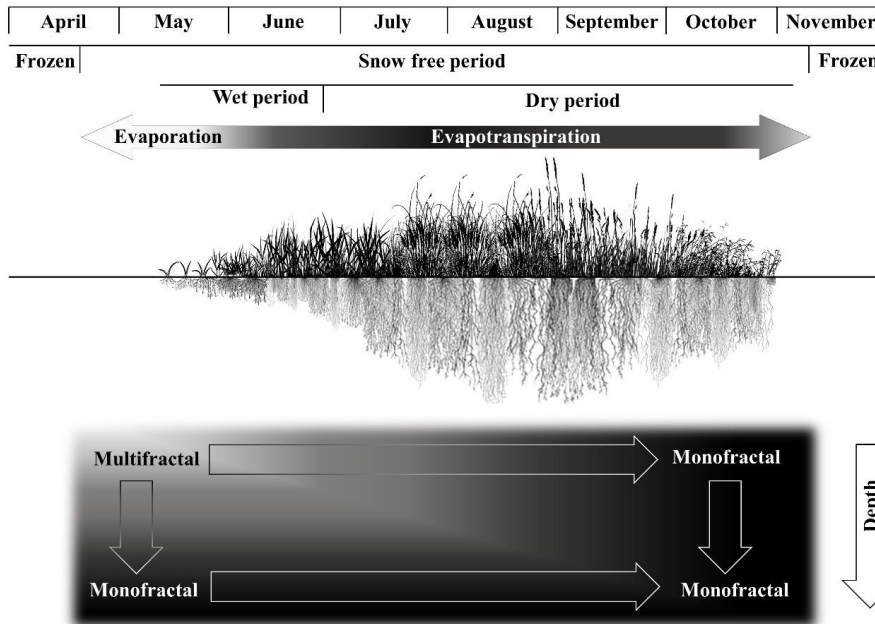
671 Figure 6
 672



673 Figure 7
 674



675
 676 Figure 8



677
 678 Figure 9